Probing low-density carriers in a single atomic layer using terahertz parallel-plate waveguides

Manjakavahoaka. Razanoelina,[1] Filchito Renee Bagsican,[1] Iwao Kawayama,[1] Xiang Zhang,[2] Lulu Ma,[2] Hironaru Murakami,[1] Robert Vajtai,[2] Pulickel M. Ajayan,[2] Junichiro Kono,[1-4] and Masayoshi Tonouchi[1,*]

[1]*Institute of Laser Engineering, Osaka University, 2-6 Yamadaoka, Suita, Osaka 565-0871, Japan*
[2]*Department of Materials Science and NanoEngineering, Rice University, Houston, Texas 77005, USA*
[3]*Department of Electrical and Computer Engineering, Rice University, Houston, Texas 77005, USA*
[4]*Department of Physics & Astronomy, Rice University, Houston, Texas 77005, USA*
[*]*tonouchi@ile.osaka-u.ac.jp*

Abstract: As novel classes of two-dimensional (2D) materials and heterostructures continue to emerge at an increasing pace, methods are being sought for elucidating their electronic properties rapidly, non-destructively, and sensitively. Terahertz (THz) time-domain spectroscopy is a well-established method for characterizing charge carriers in a contactless fashion, but its sensitivity is limited, making it a challenge to study atomically thin materials, which often have low conductivities. Here, we employ THz parallel-plate waveguides to study monolayer graphene with low carrier densities. We demonstrate that a carrier density of ~2×10^{11} cm^{-2}, which induces less than 1% absorption in conventional THz transmission spectroscopy, exhibits ~30% absorption in our waveguide geometry. The amount of absorption exponentially increases with both the sheet conductivity and the waveguide length. Therefore, the minimum detectable conductivity of this method sensitively increases by simply increasing the length of the waveguide along which the THz wave propagates. In turn, enabling the detection of low-conductivity carriers in a straightforward, macroscopic configuration that is compatible with any standard time-domain THz spectroscopy setup. These results are promising for further studies of charge carriers in a diverse range of emerging 2D materials.

OCIS codes: (310.6860) Thin films, optical properties; (230.7370) Waveguides; (300.6495) Spectroscopy, terahertz.

References and links

1. K. S. Novoselov, A. K. Geim, S. V. Morozov, D. Jiang, Y. Zhang, S. V. Dubonos, I. V. Grigorieva, and A. A. Firsov, "Electric field effect in atomically thin carbon films," Science **306**(5696), 666–669 (2004).
2. C. R. Dean, A. F. Young, I. Meric, C. Lee, L. Wang, S. Sorgenfrei, K. Watanabe, T. Taniguchi, P. Kim, K. L. Shepard, and J. Hone, "Boron nitride substrates for high-quality graphene electronics," Nat. Nanotechnol. **5**(10), 722–726 (2010).
3. M. Chhowalla, H. S. Shin, G. Eda, L.-J. Li, K. P. Loh, and H. Zhang, "The chemistry of two-dimensional layered transition metal dichalcogenide nanosheets," Nat. Chem. **5**(4), 263–275 (2013).
4. K. F. Mak, C. Lee, J. Hone, J. Shan, and T. F. Heinz, "Atomically thin MoS_2: a new direct-gap semiconductor," Phys. Rev. Lett. **105**(13), 136805 (2010).
5. S. Lei, L. Ge, Z. Liu, S. Najmaei, G. Shi, G. You, J. Lou, R. Vajtai, and P. M. Ajayan, "Synthesis and photoresponse of large GaSe atomic layers," Nano Lett. **13**(6), 2777–2781 (2013).
6. S. Lei, L. Ge, S. Najmaei, A. George, R. Kappera, J. Lou, M. Chhowalla, H. Yamaguchi, G. Gupta, R. Vajtai, A. D. Mohite, and P. M. Ajayan, "Evolution of the electronic band structure and efficient photo-detection in atomic layers of InSe," ACS Nano **8**(2), 1263–1272 (2014).
7. X. Ling, H. Wang, S. Huang, F. Xia, and M. S. Dresselhaus, "The renaissance of black phosphorus," Proc. Natl. Acad. Sci. U.S.A. **112**(15), 4523–4530 (2015).
8. P. U. Jepsen, D. G. Cooke, and M. Koch, "Terahertz spectroscopy and imaging—modern techniques and applications," Laser Photonics Rev. **5**(1), 124–166 (2011).

#253324 Received 5 Nov 2015; revised 21 Jan 2016; accepted 30 Jan 2016; published 16 Feb 2016

9. J. Horng, C.-F. Chen, B. Geng, C. Girit, Y. Zhang, Z. Hao, H. A. Bechtel, M. Martin, A. Zettl, M. F. Crommie, Y. R. Shen, and F. Wang, "Drude conductivity of Dirac fermions in graphene," Phys. Rev. B **83**(16), 165113 (2011).
10. L. Ren, Q. Zhang, J. Yao, Z. Sun, R. Kaneko, Z. Yan, S. Nanot, Z. Jin, I. Kawayama, M. Tonouchi, J. M. Tour, and J. Kono, "Terahertz and infrared spectroscopy of gated large-area graphene," Nano Lett. **12**(7), 3711–3715 (2012).
11. C. Qiu, W. Gao, R. Vajtai, P. M. Ajayan, J. Kono, and Q. Xu, "Efficient modulation of 1.55 μm radiation with gated graphene on a silicon microring resonator," Nano Lett. **14**(12), 6811–6815 (2014).
12. H. Li, Y. Anugrah, S. J. Koester, and M. Li, "Optical absorption in graphene integrated on silicon waveguides," Appl. Phys. Lett. **101**(11), 111110 (2012).
13. M. Furchi, A. Urich, A. Pospischil, G. Lilley, K. Unterrainer, H. Detz, P. Klang, A. M. Andrews, W. Schrenk, G. Strasser, and T. Mueller, "Microcavity-integrated graphene photodetector," Nano Lett. **12**(6), 2773–2777 (2012).
14. M. Engel, M. Steiner, A. Lombardo, A. C. Ferrari, H. V. Löhneysen, P. Avouris, and R. Krupke, "Light-matter interaction in a microcavity-controlled graphene transistor," Nat. Commun. **3**, 906 (2012).
15. M. Razanoelina, R. Kinjo, K. Takayama, I. Kawayama, H. Murakami, D. M. Mittleman, and M. Tonouchi, "Parallel-plate waveguide terahertz time domain spectroscopy for ultrathin conductive films," J. Infrared Millim. Terahertz Waves **36**(12), 1182–1194 (2015).
16. A. C. Ferrari, J. C. Meyer, V. Scardaci, C. Casiraghi, M. Lazzeri, F. Mauri, S. Piscanec, D. Jiang, K. S. Novoselov, S. Roth, and A. K. Geim, "Raman spectrum of graphene and graphene layers," Phys. Rev. Lett. **97**(18), 187401 (2006).
17. C.-F. Chen, C.-H. Park, B. W. Boudouris, J. Horng, B. Geng, C. Girit, A. Zettl, M. F. Crommie, R. A. Segalman, S. G. Louie, and F. Wang, "Controlling inelastic light scattering quantum pathways in graphene," Nature **471**(7340), 617–620 (2011).
18. Y.-C. Lin, C.-C. Lu, C.-H. Yeh, C. Jin, K. Suenaga, and P.-W. Chiu, "Graphene annealing: how clean can it be?" Nano Lett. **12**(1), 414–419 (2012).
19. M. Naftaly and R. Dudley, "Methodologies for determining the dynamic ranges and signal-to-noise ratios of terahertz time-domain spectrometers," Opt. Lett. **34**(8), 1213–1215 (2009).
20. D. M. Pozar, *Microwave Engineering 3e* (John Wiley & Son, 2006).
21. D. Grischkowsky and S. Keiding, "THz time-domain spectroscopy of high T_c substrates," Appl. Phys. Lett. **57**(10), 1055 (1990).
22. R. Mendis, "Nature of subpicosecond terahertz pulse propagation in practical dielectric-filled parallel-plate waveguides," Opt. Lett. **31**(17), 2643–2645 (2006).
23. K. S. Champlin and G. H. Glover, "Influence of waveguide contact on measured complex permittivity of semiconductors," J. Appl. Phys. **37**(6), 2355 (1966).
24. R. Mendis and D. M. Mittleman, "An investigation of the lowest-order transverse-electric (TE_1) mode of the parallel-plate waveguide for THz pulse propagation," J. Opt. Soc. Am. B **26**(9), A6–A13 (2009).
25. R. R. Hartmann, J. Kono, and M. E. Portnoi, "Terahertz science and technology of carbon nanomaterials," Nanotechnology **25**(32), 322001 (2014).
26. N. H. Shon and T. Ando, "Quantum transport in two-dimensional graphite system," J. Phys. Soc. Jpn. **67**(7), 2421–2429 (1998).
27. Y. Zheng and T. Ando, "Hall conductivity of a two-dimensional graphite system," Phys. Rev. B **65**(24), 245420 (2002).
28. T. Ando, Y. Zheng, and H. Suzuura, "Dynamical conductivity and zero-mode anomaly in honeycomb lattices," J. Phys. Soc. Jpn. **71**(5), 1318–1324 (2002).
29. N. M. R. Peres, F. Guinea, and A. H. Castro Neto, "Electronic properties of disordered two-dimensional carbon," Phys. Rev. B **73**(12), 125411 (2006).
30. S. A. Mikhailov, "Non-linear graphene optics for terahertz applications," Microelectronics J. **40**(4-5), 712–715 (2009).
31. Z. Q. Li, E. A. Henriksen, Z. Jiang, Z. Hao, M. C. Martin, P. Kim, H. L. Stormer, and D. N. Basov, "Dirac charge dynamics in graphene by infrared spectroscopy," Nat. Phys. **4**(7), 532–535 (2008).
32. C. Lee, J. Y. Kim, S. Bae, K. S. Kim, B. H. Hong, and E. J. Choi, "Optical response of large scale single layer graphene," Appl. Phys. Lett. **98**(7), 071905 (2011).
33. J. Y. Kim, C. Lee, S. Bae, K. S. Kim, B. H. Hong, and E. J. Choi, "Far-infrared study of substrate-effect on large scale graphene," Appl. Phys. Lett. **98**(20), 201907 (2011).
34. Y. Sano, I. Kawayama, M. Tabata, K. A. Salek, H. Murakami, M. Wang, R. Vajtai, P. M. Ajayan, J. Kono, and M. Tonouchi, "Imaging molecular adsorption and desorption dynamics on graphene using terahertz emission spectroscopy," Sci. Rep. **4**, 6046 (2014).
35. F. Schedin, A. K. Geim, S. V. Morozov, E. W. Hill, P. Blake, M. I. Katsnelson, and K. S. Novoselov, "Detection of individual gas molecules adsorbed on graphene," Nat. Mater. **6**(9), 652–655 (2007).
36. L. G. Booshehri, C. H. Mielke, D. G. Rickel, S. A. Crooker, Q. Zhang, L. Ren, E. H. Hároz, A. Rustagi, C. J. Stanton, Z. Jin, Z. Sun, Z. Yan, J. M. Tour, and J. Kono, "Circular polarization dependent cyclotron resonance in large-area graphene in ultrahigh magnetic fields," Phys. Rev. B **85**(20), 205407 (2012).
37. Z. H. Ni, H. M. Wang, Z. Q. Luo, Y. Y. Wang, T. Yu, Y. H. Wu, and Z. X. Shen, "The effect of vacuum annealing on graphene," J. Raman Spectrosc. **41**(5), 479–483 (2010).

#253324 Received 5 Nov 2015; revised 21 Jan 2016; accepted 30 Jan 2016; published 16 Feb 2016

1. Introduction

Currently, there is much interest in atomically thin, layered materials, including graphene [1], hexagonal BN [2], transition metal dichalcogenides (e.g., MoS_2, WSe_2) [3, 4], III-VI layered semiconductors (e.g., InSe, GaSe) [5, 6], and black phosphorous [7]. These novel materials host two-dimensional (2D) carriers with unconventional properties that are promising for a wide range of applications in electronics, photonics, and optoelectronics. However, many of these emerging materials have rather low conductivities, which require high-sensitivity techniques in order to reveal their basic characteristics and provide insight into their novel band structure.

In the terahertz (THz) frequency regime, the complex conductivity, σ, of charge carriers can be conveniently determined without any contacts by using THz time-domain spectroscopy (THz-TDS) [8]. However, when applied to 2D materials, conventional THz-TDS usually requires tremendous efforts to detect finite signals because of the small interaction between THz radiation and the material. Since these materials are atomically thin, a normal incident beam in a standard transmission THz spectroscopy system experiences a very short-length interaction with the material.

One of the widely used methods to increase the response of 2D materials to THz radiation is by increasing the carrier density through "gating", i.e., by applying an external electric field in a transistor configuration [9, 10]. However, this is not always possible for general 2D materials and, more importantly, requires gate electrodes. One would also have to consider possible influences of gate-induced carriers in the substrate. A more convenient approach is to integrate graphene in a planar waveguide geometry. Demonstrations have been reported about the efficiency of such a geometry in the infrared/visible range for waveguide modulators [11, 12] and in graphene-based transistors and microcavities [13, 14]. However, these waveguide hybrid structures are not suitable for THz spectroscopy applications. Primarly because most of those devices operate at a specific frequency which is the main limiting factor of their exploitation in a broadband THz-TDS.

Here, we describe a sensitive, non-destructive, and versatile method for characterizing the conductivities of atomically thin materials in the THz range using a parallel-plate waveguide (PPWG). Such an approach is particularly attractive because the long interaction length inside a waveguide provides a high sensitivity. The achievable interaction length is only limited by the waveguide length. Furthermore, waveguide geometries allow one to readily probe the response of a 2D materials to different electromagnetic polarizations (electric field parallel or perpendicular to the 2D surface) through waveguide mode control. We previously studied highly conducting thin gold films using a similar setup [15], while, in the present study, we successfully probed and characterized low-density carriers in a single atomic layer of graphene. The graphene layer was sandwiched between two MgO substrates and inserted into the PPWG. In this configuration, the interaction of the fundamental transverse electric (TE_1) mode to the graphene layer was optimal, leading to a substantial (~30%) change in transmission even for a sheet carrier density as low as 2×10^{11} cm^{-2}. On the other hand, conventional normal-incidence transmission THz-TDS failed to detect any signal for this density. Furthermore, the transverse magnetic (TM) mode did not show any sign of interaction with the graphene monolayer, as expected, since the electric field in this mode is perpendicular to the 2D layer.

2. Technique

Two graphene samples (Sample A and Sample B), grown by chemical vapor deposition (CVD), were used in this study. Copper foil was placed in the deposition chamber and annealed at a temperature of 1000°C in a hydrogen/argon gas at a pressure of 1 Torr for 20 min. Methane was introduced into the chamber with a flow rate of 4 standard cubic centimeters per minute for 10 min. The sample was cooled for 20 min. in a hydrogen/argon gas. The grown graphene layer was then transferred onto a MgO (100) substrate, which is transparent in the THz frequency range. The dimensions of the MgO substrate were 30 mm

#253324 Received 5 Nov 2015; revised 21 Jan 2016; accepted 30 Jan 2016; published 16 Feb 2016

(width) × 10 mm (length) × 0.5 mm (thickness). Half of the substrate was covered by CVD graphene. Raman spectra at different spots of the sample confirmed the single-layer nature of graphene. The intensity ratio of the G mode to the 2D mode in Raman spectra confirmed that monolayer graphene was grown (Fig. 1) [16]. The Fermi energy, E_F, of the grown sample was also calculated from the G-mode peak position, ω_G, using the formula ω_G (cm^{-1}) = 1580 (cm^{-1}) + $|E_F|$ (eV) × 42 ($cm^{-1}eV^{-1}$) [17].

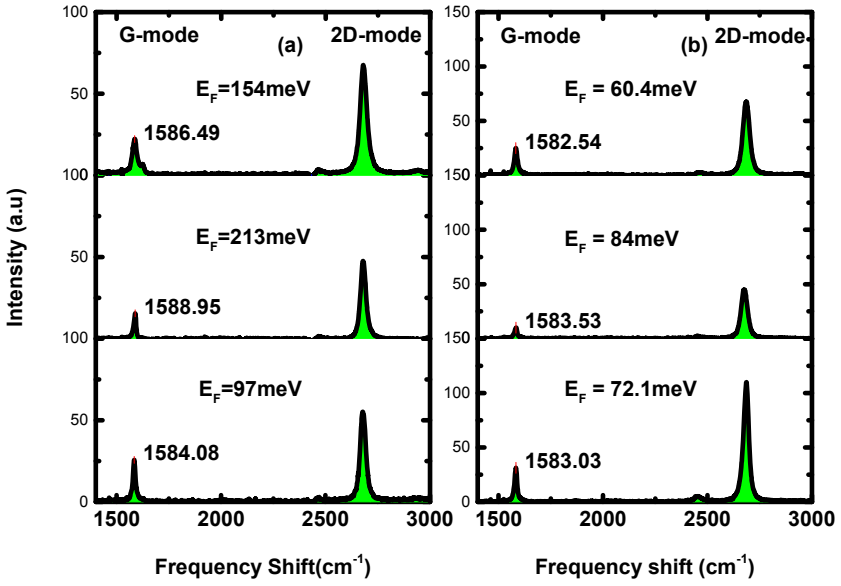

Fig. 1. Raman Spectra of graphene samples and associated Fermi energies associated. Each Raman spectrum represents one location in the graphene side of the sample. The frequency position of G-mode peaks are also shown. The difference in intensities is due to the difference of the laser pump power used in Raman spectroscopy. The unit of the frequency shift inside the figures is cm^{-1}. (a). Raman spectra of sample A before annealing. (b). Raman spectra of sample A after annealing

Figure 2 shows a schematic illustration of the PPWG system used in this study. We used a waveguide made of two aluminum plates. The area of the aluminum plate surfaces was the same as that of the MgO substrate (30 mm × 10 mm). We inserted the substrate with graphene and another bare substrate on top of it inside the PPWG. Therefore, the separation between the waveguide plates was around 1 mm. The PPWG was set at the center of a four-parabolic-mirror system. The THz emitter was p-type InAs excited by an 800-nm beam from a Ti:sapphire laser at a repetition rate of 80 MHz. A wire-grid polarizer was placed before the waveguide to control the polarization of the input THz beam. The THz input beam diameter was roughly measured with pinhole at the maximum electric field. The beam spot diameter was approximately 3mm. The experimental system was placed in a dry nitrogen environment to avoid water vapor absorption. The waveform transmitted through the other half part of the waveguide, in which two MgO substrates with no graphene were inserted, was used as the reference. Further details have been reported elsewhere [15]. Characterization measurements of each graphene sample were performed in two steps. First, we characterized the sample using PPWG THz-TDS. Then, the MgO substrate with graphene sample was removed from the waveguide assembly and placed in a cryostat. We annealed the sample at 445 K under a pressure of ~10^{-7} Torr for one hour [10, 18], followed by cooling for about four hours in the vacuum chamber, after which we immediately measured the sample again with PPWG THz-TDS.

#253324 Received 5 Nov 2015; revised 21 Jan 2016; accepted 30 Jan 2016; published 16 Feb 2016

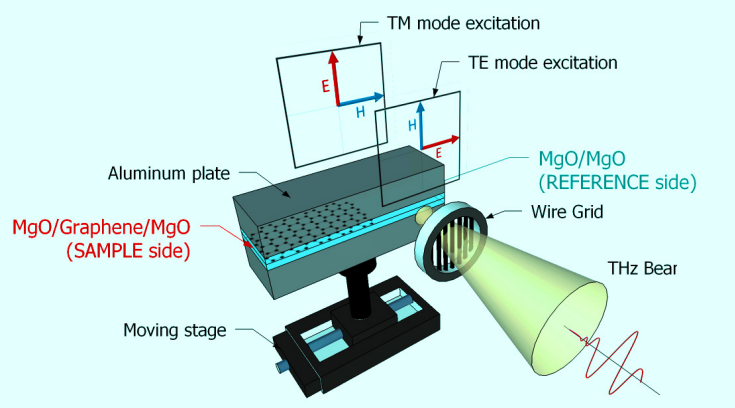

Fig. 2. PPWG THz-TDS setup. The input electric field of the THz beam is polarized parallel (perpendicular) to the waveguide plates to excite TE (TM) mode by mean of wire grid polarizer. Here, the plate separation is determined by the thickness of the two MgO substrates (~1 mm). Then, the cutoff frequency for the fundamental TE mode (TE_1) is 0.06 THz while the fundamental TM mode has no cutoff frequency. The PPWG device is mounted on a controlled mechanical stage in order to move it in small steps (~1.5 mm) in the direction perpendicular to the THz wave propagation direction. For averaging purposes, ten time-domain THz waveforms were recorded for each of the reference side (PPWG without graphene) and the sample side (PPWG with graphene).

Figure 3 shows typical fast Fourier transform amplitude spectra corresponding to the time-domain THz waveforms shown in the inset of Fig. 3. The THz wave was TE-polarized, and the spectra were taken for Sample A before annealing. For PPWG THz TDS, we found that the accuracy of data was affected more by waveguide alignment than by the signal-to-noise ratio (SNR) of the low-temperature-grown GaAs detector. In order to take account of the non-uniformity coverage of the sample and misalignment effects of the waveguide, THz reference pulses and sample pulses are, respectively, recorded in ten different locations. Then, according to the definition in [19], the SNR associated with the spectra was determined by the ratio of the mean value of THz spectrum amplitudes (10 spectra on the reference side) to its standard deviation.

We fitted the experimental data with a multimodal transfer function [15]. TE and TM mode dispersion equations were used to evaluate the propagation constant and the waveguide loss as a function of the sheet conductivity of the sample. Here, the absence of interferences in the experimental frequency-domain THz spectra (Fig. 3) suggests that single-mode propagation is realized. Then, in the frequency (ν) domain, the complex transmittance coefficient is defined as

$$\tilde{T}(\nu) = \frac{\tilde{E}_{\mathrm{MgO/Gr/MgO}}}{\tilde{E}_{\mathrm{MgO/MgO}}} = \left|\tilde{T}\right| e^{j\Delta\varphi} = e^{-j\Delta\gamma L} \tag{1}$$

where $\tilde{E}_{\mathrm{MgO/Gr/MgO}}$ is the complex frequency-dependent electric field detected through the waveguide with graphene, $\tilde{E}_{\mathrm{MgO/MgO}}$ is the electric field detected without graphene, $\Delta\varphi$ is the experimental phase difference between the reference and the sample pulses, $\Delta\gamma \equiv \Delta\beta - j\Delta\alpha$, β is the propagation constant of the PPWG mode under consideration (TE or TM mode), and α is the propagation loss. The length of the waveguide, L, is 10 mm. Note that Eq. (1) works only for single-mode propagation, either in the TE mode or TM mode.

#253324 Received 5 Nov 2015; revised 21 Jan 2016; accepted 30 Jan 2016; published 16 Feb 2016

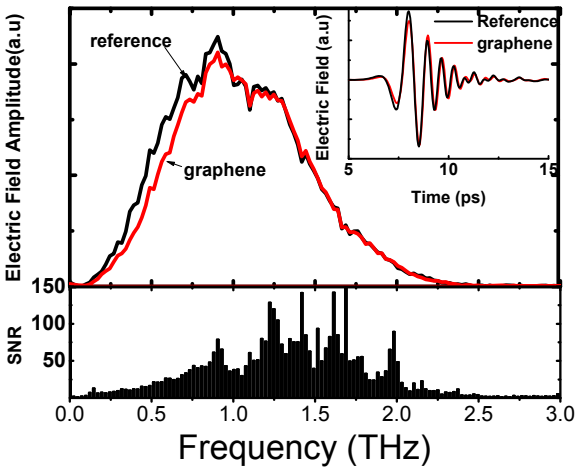

Fig. 3. THz spectra of the reference and Sample A (top panel) with an associated SNR spectrum of the system (bottom panel). The inset shows typical time-domain waveforms of detected THz radiation in the TE mode for the reference and sample signals. The spectra of reference (black curve) and sample (red curve) were obtained after averaging over ten spectra. The absence of any obvious interference fringes in the frequency domain ensures single-mode propagation. The small dips are due to remaining water vapor in the system. The small values of SNR at low and high frequencies are due to the detection limit of the low-temperature-grown GaAs photoconductive antenna receiver used.

Using waveguide theory with appropriate boundary conditions [15, 20], we find the sheet conductivity in the TE mode to be

$$\sigma_s(\nu) = j\frac{\sqrt{4\pi\nu^2\mu\varepsilon_0 n_{\mathrm{MgO}}^2 - \gamma^2}}{\pi\nu\mu}\cot\left(\sqrt{4\pi\nu^2\mu\varepsilon_0 n_{\mathrm{MgO}}^2 - \gamma^2}\,\frac{d}{2}\right), \qquad (2)$$

where ν, μ, ε_0, n_{MgO}, d are, respectively, the frequency, the substrate permeability, the vacuum permittivity, the refractive index of MgO in the THz region (3.15 ± 0.05) [21], and the PPWG plate separation, which is fixed by the substrate thickness. All MgO substrates used in this experiment had a thickness of 0.5 ± 0.015 mm; thus, we set d = 1 mm for all parameter extraction processes. Equation (2) can be used to deduce the real and imaginary parts of the graphene THz sheet conductivity.

We notice that Eq. (2) was derived for the case of ideal contact of the interfaces between the substrate and the PPWG plates. However, it has been reported that sub-micron air gaps in the contact interfaces between the dielectric slab and the metal plates, dramatically affects the THz pulse of the fundamental transverse electromagnetic mode (TEM) [22]. In the particular case of TE_1 mode, the air-gap effect is less important since the electric field is zero along the PWWG walls [23].

3. Results and discussion

We first compare spectra collected by the conventional transmission THz-TDS and the PPWG THz-TDS. Figure 4 shows transmittance spectra for Sample A taken by both methods. In the case of conventional THz-TDS, the spectra are nearly flat over the entire frequency range for both before and after annealing, with transmittance ~95% and ~98%, respectively. It should be noted that each transmission curve taken by conventional THz-TDS was averaged over 20 spectra. In the case of PPWG THz-TDS, the transmittance clearly shows some frequency dependence. The transmittance value is ~60% (~70%) before (after) annealing in the low-frequency region while it increases to ~95% at the high-frequency end of the spectra. These results definitevely demonstrate the advantage of using PPWG TDS.

#253324 Received 5 Nov 2015; revised 21 Jan 2016; accepted 30 Jan 2016; published 16 Feb 2016

If the fundamental TE mode (TE_1) of the bare PPWG does not change much in the presence of graphene, a perturbation method [20] simplifies Eq. (1) to $|T| \approx \exp(-C\sigma_S L)$, where C is a constant. From this expression, we see two important features of PPWG THz-TDS. First, a longer waveguide yields exponentially stronger absorption and thus a higher sensitivity. Second, the transmission decreases exponentially with increasing sheet conductivity; thus, tiny differences in conductivity substantially change transmission. These advantages of PPWG THz-TDS are demonstrated in Fig. 4.

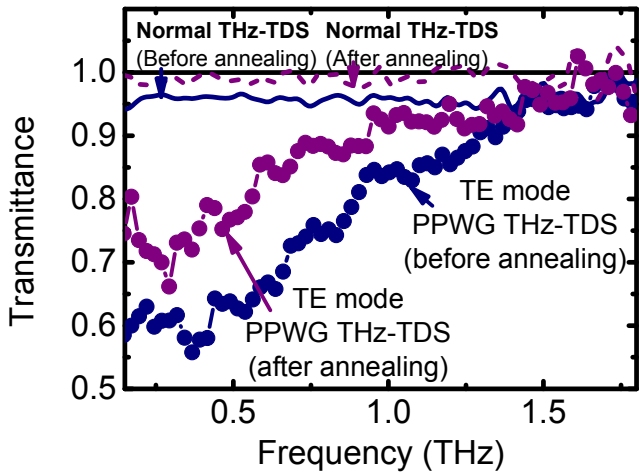

Fig. 4. Comparison of normal-incidence transmission THz-TDS and PPWG THz-TDS transmittance in TE mode. (Sample A before and after annealing). The upper quasi-flat curves are averaged transmittance data taken with THz-TDS. The blue solid curve is for non-annealed graphene on MgO and the purple dashed curve is for annealed graphene on MgO. The same sample is analyzed with waveguide in TE mode, leading to a frequency-dependent transmittance represented by blue solid circles for Sample A before annealing and by purple solid circles for after annealing.

From the perspective of mode propagation, we can consider the TE mode as a propagating plane wave bouncing between the waveguide plates with polarization parallel to the layer surface [24]. Due to the frequency cutoff of the TE_1 mode ($\nu_c \approx 0.06$ THz), the free-space THz pulse is reshaped when traveling through the waveguide (inset of Fig. 3), and the phase and group velocities become strongly frequency dependent. Lower-frequency components of the THz wave traverse the waveguide more slowly than higher-frequency components and hence experience a larger number of bounces. An increase in the number of bounces yields stronger absorption by the sample. Therefore, this dispersive nature of TE_1 mode provides a more efficient approach to the study of weakly conducting material. This fact is counterintuitive in THz spectroscopy since it is usually common to avoid such dispersion.

We also performed TM mode analysis of graphene in a PPWG. The two spectra of reference and sample (not shown here) overlap each other over the entire frequency range. Namely, the system is not capable of separating the sample absorption of the THz wave from other sources of uncertainty (e.g., misalignment, SNR of the detector). In fact, in a real 2D material like graphene, the electrons are confined in the sample plane. Consequently, when an electric field perpendicular to the surface (TM mode) is applied to the sample, there is no current induced, and thus, there is no THz absorption. The conductivity is zero in that direction.

Microscopically, the optical response of graphene in the THz range is mainly dominated by intraband free-carrier absorption [9, 10, 25], describable by the Drude formula [26–31]

#253324 Received 5 Nov 2015; revised 21 Jan 2016; accepted 30 Jan 2016; published 16 Feb 2016

$$\sigma_S = \frac{jD}{(2\pi\nu + j\Gamma)} \tag{3}$$

where Γ is the scattering rate and the Drude weight D is given by

$$D = \frac{e^2 k_B T}{\pi\hbar^2} \ln\left(2\cos h \frac{E_F}{2k_B T}\right). \tag{4}$$

Here, e is the electronic charge, $\hbar$ is the reduced Planck constant, k_B is the Boltzmann constant, and T is the temperature.

Figure 5 shows an example of the real and imaginary parts of the sheet conductivity for Sample A before annealing, together with fitting curves using the Drude formula. The conductivity is expressed in units of σ_0, where $\sigma_0 = \pi e^2/2h \approx 6.1 \times 10^{-5}$ S is the universal interband conductivity of graphene [28, 30, 31]. From the relation between E_F and the carrier concentration N [31], we found $N = 1.07 \times 10^{12}$ cm^{-2} for Sample A and $N = 1.01 \times 10^{12}$ cm^{-2} for Sample B before annealing. The scattering rate obtained were $\Gamma = 3.39 \times 10^{12}$ s^{-1} for Sample A and $\Gamma = 4.2 \times 10^{11}$ s^{-1} for Sample B. These values are comparable with reported values for CVD-grown graphene on different substrates [9, 10, 32, 33].

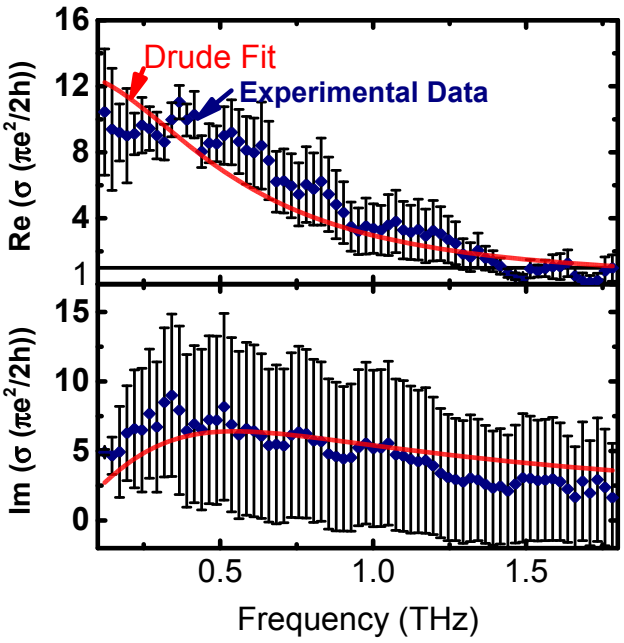

Fig. 5. Drude model fit of the graphene conductivity (Sample A before annealing). The blue diamonds are the mean values of experimental conductivity, and the error bars represent the standard deviation. The red curve is the theoretical Drude fit while the frequency range used for the fitting process was set to be 0.1-1.8 THz.

Table 1 shows the fitting parameters of the Drude model extracted from the experimental data for both Sample A and Sample B: scattering rate, Γ (s^{-1}), carrier density, N (cm^{-2}), and Fermi Energy, E_F (meV). It has been experimentally observed that adsorption of water and oxygen molecules dramatically changes the electromagnetic properties of graphene [10, 34]. In fact, transport measurements [35] revealed that charge transfer occurs between adsorbed molecules and graphene. Vacuum annealing described in the experimental section removes these adsorbed molecules [36] and additionally reduces PMMA residues and other impurities

#253324 Received 5 Nov 2015; revised 21 Jan 2016; accepted 30 Jan 2016; published 16 Feb 2016

[37]. It can indeed be seen in Table 1 that the annealing process reduces the carrier density ($N = 2.3 \times 10^{11}$ cm^{-2} for Sample A and $N = 2.2 \times 10^{11}$ cm^{-2} for Sample B). These small numbers of densities were accurately determined by the PPWG THz-TDS method while normal THz-TDS could not detect any THz absorption after annealing, as also shown in Table 1 for Sample A.

Table 1. Drude fitting parameters extracted for Samples A and B before and after annealing using parallel-plate waveguides (PPWG) and conventional THz-TDS

	Sample A			Sample B	
	Before annealing		After annealing	Before annealing	After annealing
	PPWG	THz-TDS	PPWG	PPWG	PPWG
$\Gamma(10^{12}$ s$^{-1})$	3.39	5.84	2.6	4.2	4.08
N (10^{12} cm^{-2})	1.07	1.94	0.23	1.01	0.22
E_F (meV)	133	179	62.1	129	61

Conclusion

In summary, we have demonstrated that parallel-plate waveguide based THz spectroscopy is a powerful technique for characterizing 2D materials, using graphene as an example. This method has particular advantages at low frequencies due to longer interaction paths between the propagating THz wave and the 2D material, leading to a better sensitivity than the conventional THz spectroscopy techniques. Using this waveguide approach, we observed a substantial (~30%) change in transmission even for a sheet carrier density as low as 2×10^{11} cm^{-2} whereas conventional normal-incidence transmission THz spectroscopy did not produce any signal for this low density.

Acknowledgments

This work was partially funded by Grant-in-Aid for Scientific Research (No. 25630149 and No. 26107524), JSPS/MEXT, Air Force Office of Scientific Research (AFSOR) (grant number FA9550-14-1-0268 and FA2386-15-1-0004), and Program for Promoting International Joint Research, Osaka University. The authors are grateful to Cody Sewell of Rice University for comments and dicussions.

#253324 Received 5 Nov 2015; revised 21 Jan 2016; accepted 30 Jan 2016; published 16 Feb 2016